Multi-Parametric Condition Monitoring of Medium-Power Generators with Brushless Exciters under Mechanical Faults

Konstantinos N. Gyftakis, *Senior, IEEE*, Carlos A. Platero, *Senior, IEEE*, and Jonas K. Nøland, *Senior, IEEE*

***Abstract*—The interest in reliable condition monitoring of small-to-medium-power generator sets (GenSets) has increased in recent years due to the multiple benefits of prompt and decisive fault detection. This leads to the minimization of catastrophic failures and significantly improves the interconnected load's power reliability. In this paper, the case of mechanical faults is examined and particularly the eccentricity caused by a cocked bearing. The main electrical machine under investigation is a salient pole wound-field synchronous machine (WFSM) with a brushless exciter (BE), which is a very common topology in GenSets. The work is based purely on experimental testing, while a plethora of methods has been assessed based on their accuracy to detect and identify the fault, both stationary and dynamic. Finally, the paper proposes a new and non-intrusive method based on the monitoring of the stray leakage flux and its analysis while the generator experiences a deaccelerating transient, and the role of the exciters's geometrical properties in this new methodology is revealed.**

***Index Terms*—Condition monitoring, Eccentricity, Fault diagnosis, Synchronous machines**

I. INTRODUCTION

SMALL-TO-MEDIUM-SIZE wound-field synchronous machines (WFSMs) are preferably equipped with a brushless excitation system configured as an inside-out synchronous machine feeding a rotating diode bridge rectifier [1]. However, for starter/generator (S/G) applications, the brushless exciter is asynchronous, allowing excitation from stand-still [2].

There is a wide variety of faults that might occur in these WFSM-based generator sets, either on the exciter or the main machine. The occurrence of electrical or mechanical faults might influence the electrical characteristics of both machines. In the brushless exciter, faulted diodes are the most common electrical fault, where spectral analysis of the main machine's output voltage has been proposed to classify them [3].

Moreover, in reference [4], it is proposed to install a magnetic field sensing coil in the stator iron yoke of the brushless exciter to detect open-diode faults. The flux coil monitors the DC-current magnetic field penetrating the field-wound stator, which also interacts with the load nature of the main WFSM through the diode bridge rectifier. Even though the approach is simple and reliable, it is still an invasive approach to existing off-the-shelf solutions.

Another proposed intrusive approach is to track the air gap rotating magnetic field for detection of stator and rotor turn-to-turn faults [5]-[6], where spectral components are used for classification. For the rotor turn-to-turn fault, an invasive low-voltage AC source is suggested to be applied over the rotor field winding in offline conditions [7]. For online short-circuit fault intrusive condition monitoring, machine learning to the air gap magnetic field spectral components is applied [8]. A search coil has been inserted into the stator slot to detect broken damper bar faults in WFSMs via the air gap field [9] but also to classify field winding faults [10]. In order to make it easier for implementation, a non-intrusive axial and radial flux search coil has been proposed [11]. Alternatively, a non-invasive search coil has been suggested to capture the stray flux at the back side of the stator yoke to detect broken damper bars as well [12]. The magnetic flux monitoring has known tremendous interest and advancement lately, as shown by recent review works [13]-[14]. There are various advantages in using it for fault detection, such as the low cost, easy implementation (especially when the stray flux is monitored), independency from the electrical machines' stator windings configuration, ability to be applied online and real time, during the operation of the machines.

Similarly to the broken damper bars, turn-to-turn faults in the WFSM and diode faults in the brushless exciter, the mechanical fault would also affect the flux signature of the overall system, which is detectable by signature analysis. Over a wide range of electric fault types, mechanical effects will also be reflected, which leads to worsening the electrical asymmetries further. It is, therefore, inevitable that mechanical faults will similarly influence electrical integrity. In the opposite direction, unbalanced air gap magnetic flux densities correlate with armature winding faults (including the rotating diode bridge) in

K. N. Gyftakis is with the School of Electrical and Computer Engineering, Technical University of Crete, Chania, 73100, Greece (e-mail: k.n.gyftakis@ieee.org).

C. A. Platero are with the Electrical Machines Laboratory at ETSII Universidad Politécnica de Madrid, Madrid, Spain. (e-mail: carlosantonio.platero@upm.es)

J. K. Nøland is with the Norwegian University of Science and Technology (NTNU), Trondheim, Norway (e-mail: jonas.k.noland@ntnu.no)

both the exciter and the main WFSM, with the potential of causing UMP in both machines, which could be detected with vibration sensors. Therefore, mechanical detection is an alternative to electrical detection during electrical faults. Similarly, electrical detection is a way to monitor mechanical faults as well.

The objective of this paper is to explore the ability of accurately monitoring of mechanical faults in WFSM-based generator sets equipped with brushless exciters employing different monitoring approaches, including stator current signature analysis, leakage (SCSA, i.e., MCSA in motors), stray flux spectral analysis, and thermography, respectively. An overall sketch of the test platform [24] is depicted in Fig. 1. The remainder of the paper is organized according to the following structure. Section II describes the experimental setup. Then, Section III presents the condition monitoring analysis for the steady state. Finally, thermography is showcased as a supplementary approach in Section IV before Section V presents the transient analysis for the condition monitoring.

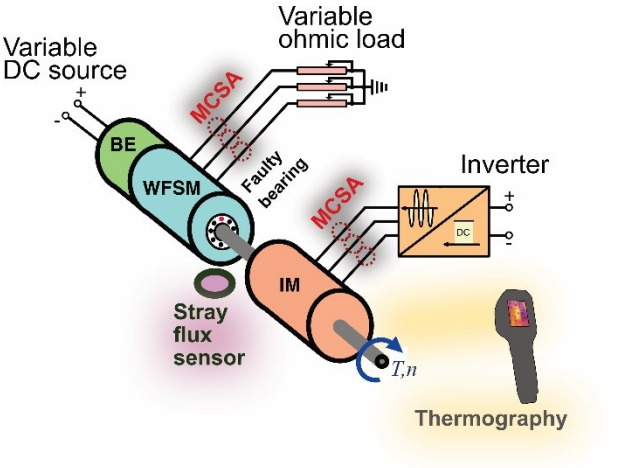

Fig. 1. Sketch of the whole generator set including prime mover (induction motor), wound-field synchronous machine (WFSM) and brushless exciter (BE), indicating the plethora of methods used to diagnose the mechanical fault, i.e., MCSA, leakage stray flux spectral analysis and thermography.

II. Description of the Experimental Setup

The experimental testing was performed on two identical salient pole WFSMs equipped with brushless exciters. The nameplate and geometrical parameters of these generators are shown in Table I. Each machine is mechanically coupled to an inverter-fed, 2-pole, 400 V, 4 kW cage induction motor, which plays the role of the prime mover. The generators have a self-magnetized shunt-connected brushless exciter as per Fig. 2, which is a very common configuration for WFSMs up to 700 kVA. However, the stator input of the exciter has been replaced by an ideal variable DC source to allow for more flexibility in conducting measurements under arbitrary excitation levels. These generator sets are usually designed to feed mainly passive ohmic-inductive loads [1]. Therefore, to emulate their natural loading condition, each WFSM was electrically connected to a symmetrical variable resistance bank that absorbs the produced electric power and plays the role of the variable load.

With respect to the measured signals, the stator currents are measured with current clamps on the load side (i_a, i_b, and i_c). Moreover, the current of the exciter (i_f) is recorded as well. Finally, a flux sensor is installed on the main body of the generator to capture the stray leakage flux (ϕ_l). Based on its position, the flux sensor measures the vector sum of the radial flux component ($\phi_{l,r}$) together with a weaker axial flux component ($\phi_{l,z}$). The flux sensor is a rigid coil around an insulating body in the form of a rectangular and has 3500 turns (N_c). All the time-varying waveforms are recorded via a data logger and stored for signal processing and analysis. The test bed is shown in Fig. 3. Moreover, the brushless exciter is presented in Fig. 4-a. The rotating part of the exciter consists of an iron core with slot number $N_e = 30$ (Fig. 3-b) hosting the exciter windings connected to the field winding via diodes.

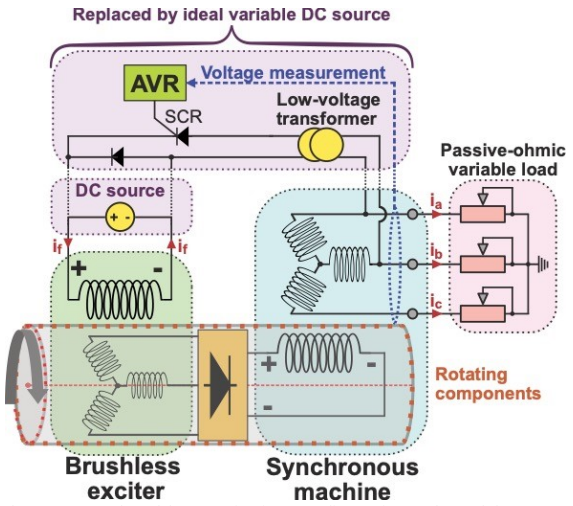

Fig. 2. The WFSM's brushless excitation configuration, adapted from [1].

One of the two WFSMs has suffered from a cocked bearing from the prime mover's side; thus, some level of eccentricity is introduced, while the other WFSM is kept healthy for comparison reasons.

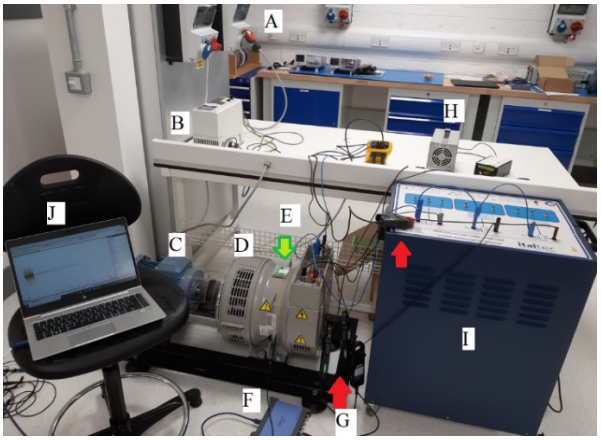

Fig. 3. The experimental test bed consisting of: A) Grid 3-phase supply, B) inverter, C) IM, D) WFSM, E) Stray flux sensor (green arrow), F) Data logger, G) Current clamps (red arrows), H) Variable DC supply, I) 3-phase Ohmic Bank and J) Data storage and analysis.

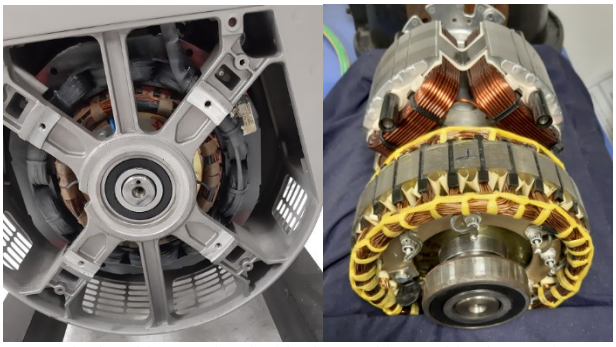

Fig. 4. a) The brushless exciter inside the machine and b) the rotating part of the exciter together with the salient pole rotor.

TABLE I
NAMEPLATE AND GEOMETRICAL PARAMETERS OF THE TESTED WFSMS

Symbol	Quantity	Value
S	rated apparent power	7.5 kVA
P	rated active power	6 kW
I_s	nominal stator current (rms)	10.8 A
U_s	nominal stator voltage (rms)	400 V
f_s	stator frequency	50 Hz
$2p$	number of poles	4
$cos(\varphi)$	power factor	0.8
U_{fr}	rated excitation voltage	52 V
I_{fr}	rated excitation current	2.2 A
L_{act}	active length	7 cm
L_{SM}	synchronous machine length	38 cm
D_{st}	outer stator diameter	26 cm
D_{rot}	outer rotor diameter	17 cm
L_{ISM}	Induction-synchronous machine distance	18 cm

III. CONDITION MONITORING AT STEADY STATE

The first set of tests was carried out while the system was in a steady state. The Motor Current Signature Analysis (MCSA) [15] has been applied to both machines to establish an overall understanding of the health state of the system. The stator current analysis has been extensively used for all types of electrical machines and faults detection. Specifically for synchronous machines, it has been applied for eccentricity detection [16]-[17], stator-inter-turn faults [17]-[18], demagnetization [17]-[19] and sensor faults [20].

In this work, the generator has been operated under reduced loading conditions (1/6 of the nominal) for safety reasons, as higher loading was observed to lead to increased vibrations and noise. Since this is a synchronous generator and the speed is fixed, a higher load would cause a higher current and operation at a higher point on the magnetic characteristic, so any triplet harmonics in the signals and associated fault harmonics would only be stronger.

It was important to make sure that the cocked bearing of the generator led to an actual shaft oscillation. For this purpose, the induction motor driving the generator was tested with the use of the MCSA. The spectra of the induction motors are shown in Fig. 5. A mixed eccentricity harmonic located at $f_s - \frac{(1-s)f_s}{p}$ is clearly seen in the faulty case and is characterized by a significant amplitude (-30.2 dB). This harmonic is absent in the healthy system. The analysis of the induction motor's stator current verifies that the cocked bearing of the WFSM has indeed introduced a significant shaft misalignment in the electromechanical system.

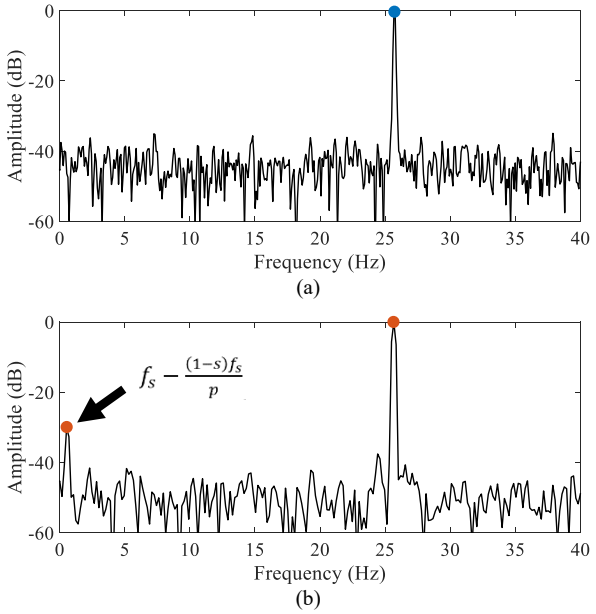

Fig. 5. Application of the MCSA on the induction motor prime mover coupled with the: (a) healthy and (b) faulty WFSM.

Furthermore, the MCSA has been applied to the WFSMs as well. The results are presented in Fig. 6. Multiple harmonics increase in the stator current spectrum. The respective amplitudes of the observed harmonics have been gathered in Table II and bar-plotted in Fig. 7.

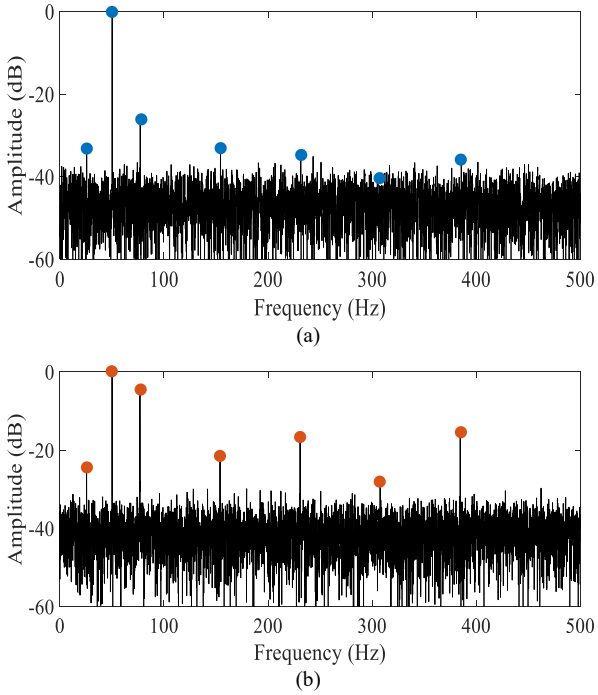

Fig. 6. Application of the MCSA on the: (a) healthy and (b) faulty WFSM.

The mechanical frequency components increase in amplitude and therefore suggest the existence of a mechanical abnormality

in the machine. It is interesting though that the main eccentricity and misalignment harmonic at $f_s - \frac{f_s}{p}$ is not the dominant one in the spectrum of the faulty machine. The harmonic with the greatest amplitude increase is the $f_s + \frac{f_s}{p}$ (>20dB). The other higher harmonics present amplitude increases between 10 and 20 dB.

Finally, the FFT spectra of the leakage stray flux (ϕ_l) at steady state have been calculated for both WFSMs and presented in Fig. 8. There are no representative harmonic increases to be detected. It is clear at this stage that, the use of the stray flux is incapable of reliable fault detection and could lead to a false negative diagnostic alarm.

TABLE II
MCSA HARMONICS AMPLITUDES OF HEALTHY AND FAULTY WFSMS

Harmonic	f_s -f_s/p	f_s +f_s/p	$3f_s$	$3f_s$ +$3f_s/p$	$6f_s$	$6f_s$ +$3f_s/p$
Frequency (Hz)	25.7	76.9	153.9	230.7	307.7	384.7
Healthy (dB)	-33.6	-26.8	-33.8	-35.3	-42.2	-37.0
Faulty (dB)	-25.0	-5.2	-22.2	-17.3	-28.3	-15.4
Deviation (dB)	+8.6	+21.6	+11.6	+18.0	+13.9	+21.6

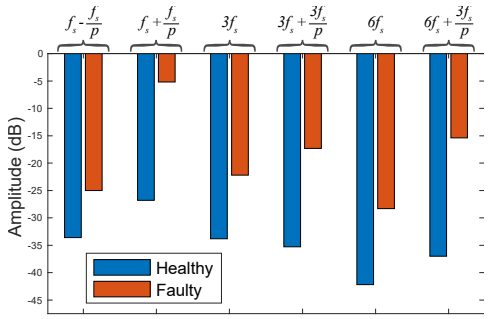

Fig. 7. Bar plot of MCSA harmonics amplitudes of healthy and faulty WFSMs.

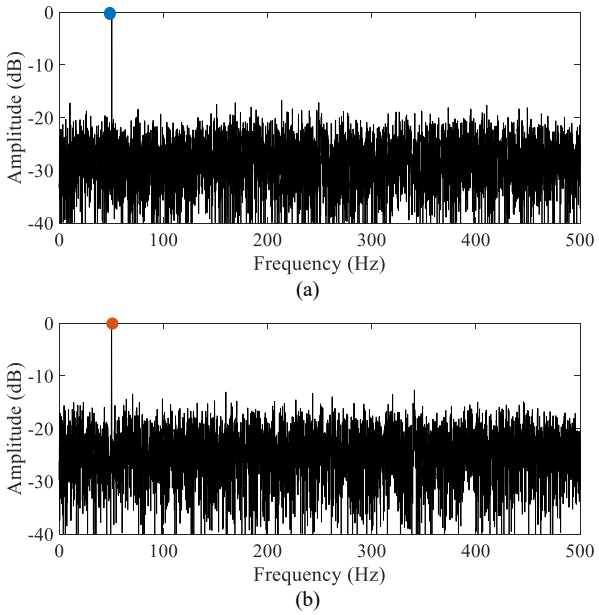

Fig. 8. FFT spectra of the leakage stray flux (ϕ_l) at steady state of the: (a) healthy and (b) faulty WFSM.

This may be due to the high noise level, which does not allow a clear overview of the higher harmonic index of the signals.

IV. THERMOGRAPHY

Thermography has been proposed in recent years as a supplementary condition monitoring method providing localization of faults and, in some cases, allowing to discriminate between different faults (mainly mechanical) [21]-[23]. Thermography is used in this paper to compare the thermal distribution between the healthy and the faulty machine. The testing of the two machines happened in parallel after they were both set to operate at steady state for one hour (1 h) to reach thermal stability. The ambient temperature of the lab is controlled and fixed during the thermal measurements.

The inner side of the cocked bearing location for the prime mover side is shown in Fig. 9 for both WFSMs. It is clear that the fault has caused additional friction leading to an increase in the temperature. The temperature difference is 2.4°C. Moreover, the thermal distribution on the other side of the SMs (brushless exciter side) has also been recorded and presented in Fig. 10. Interestingly, there is also a temperature difference of 1.3°C in favor of the faulty machine clearly showing that the mechanical oscillations are affecting the other side of the WFSM as well. Despite that, when the cover was removed, the temperature difference proved to be much greater (=3.6°C) to the prime mover side, as shown in Fig. 11. That is due to the combined effect of additional friction at the bearing due to the eccentricity as well as extra losses of the exciter due to the asymmetry. A summary of the thermal imaging maximum temperatures for the respective cases is presented in Table III.

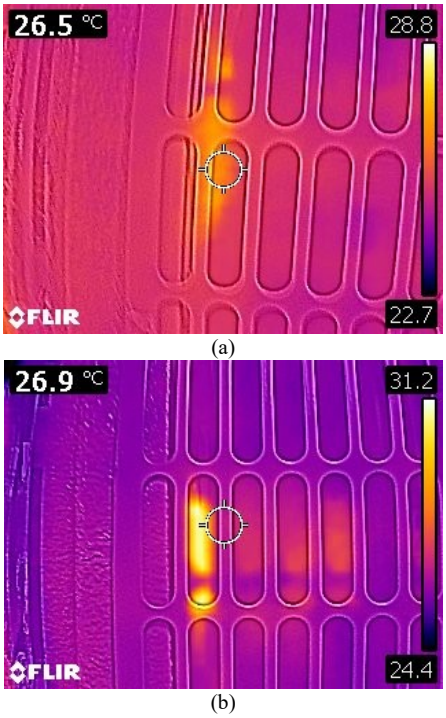

Fig. 9. Thermal imaging of the interior side of the cocked bearing located at the prime mover side of the: (a) healthy and (b) faulty WFSM.

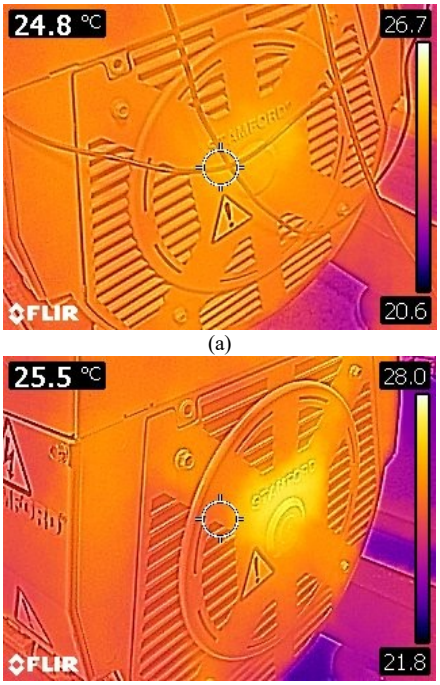

Fig. 10. Thermal imaging of the brushless exciter side of the: a) healthy and b) faulty WFSM.

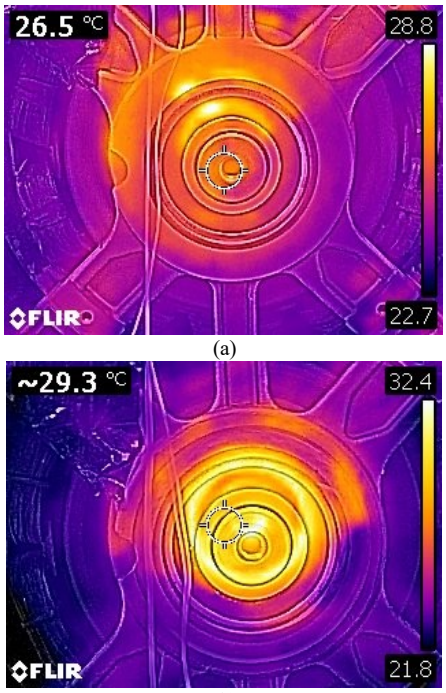

Fig. 11. Thermal imaging of the brushless exciter side after removing the protecting cover of the: (a) healthy and (b) faulty WFSM.

V. Condition Monitoring During Transients

A. *Flux Monitoring on the SM Steel Frame*

The transient operation consists of an immediate shut down of the prime mover while the system operates at steady state.

TABLE III
THERMAL IMAGING MAX. TEMPERATURES OF HEALTHY AND FAULTY WFSMS

Harmonic	Prime mover side	Brushless exciter side	Brushless Exciter side without cover
Healthy (°C)	28.8	26.7	28.8
Faulty (°C)	31.2	28.0	32.4
Deviation (°C)	+2.4	+1.3	+3.6

The excitation current of the exciter is constant. The stray flux and stator current waveforms have been recorded during the rotor deceleration and its spectrogram has been calculated with the use of the Short Time Fourier Transform (STFT). The sampling frequency is 10 kHz and a Hanning window has been used to minimize the spectral leakage. Two out of four conditions are shown here. Firstly, the armature winding of the WFSM is open, and secondly, the generator feeds the ohmic load bank. The analysis results are presented in the following Figs. 12 -17.

Firstly, the stator current spectrograms are calculated when the WFSMs are under load conditions, as shown in Fig. 12. The current consists of the fundamental alone, thus not offering any fault detection capabilities.

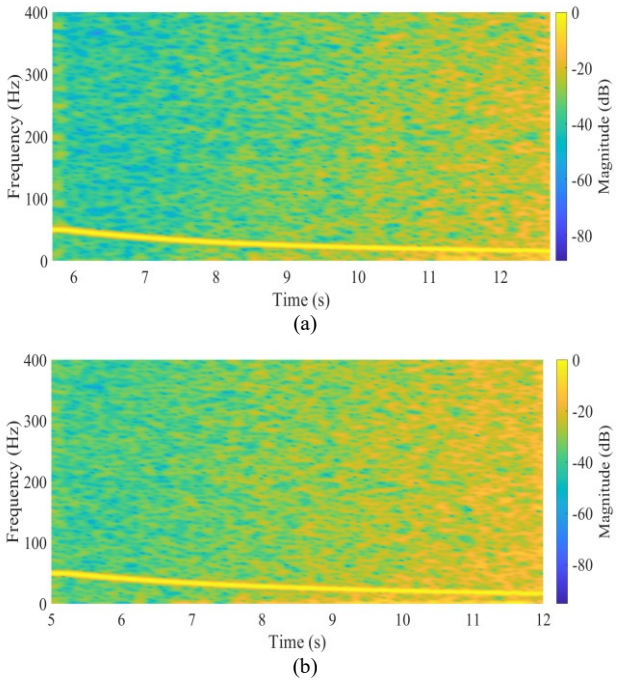

Fig. 12. Stator current STFT spectrogram when armature winding is feeding the ohmic load bank for: (a) the healthy machine and (b) the faulty machine.

The stray flux sensor is monitoring various components of the magnetic flux. Specifically, it will detect a component of the leakage and useful flux of the stator. Moreover, since the useful flux links the rotor with the stator, it will contain information of the rotor magnetic field. The stator MMF will be:

$$\mathcal{F}_m(\theta,t)=\sum_{n=2m+1}^{\infty} F_s\cos(np\theta-n\omega_s t-\varphi_n) \quad (1)$$

It is important to note that the odd triplets will pass on the stray flux as the sensor does not have a 3-phase dependence such as the one of the stator currents.

The air-gap permeance under fault will be of the following form, where the fixed part is for a symmetrical air-gap and the other part due to the dynamic variation of it with the rotor radial frequency ω_r.

$$\Lambda_{AG}(\theta,t)=\Lambda_0+\Lambda_{ecc}\sum_{k=1}^{\infty}\cos(k\theta-k\omega_r t) \quad (2)$$

The magnetic flux density, due to the interaction of (1) and (2) will be as follows:

$$B(\theta,t)=\Lambda_0\sum_{n=2m+1}^{\infty}F_s\cos(np\theta-n\omega_s t-\varphi_n)+\frac{\Lambda_{ecc}}{2}\sum_{n=2m+1}^{\infty}\sum_{k=1}^{\infty}F_s\left\{\cos\left[(np-k)\theta-\left(n-\frac{k}{p}\right)\omega_s t-\varphi_n\right]+\cos\left[(np+k)\theta-\left(n+\frac{k}{p}\right)\omega_s t-\varphi_n\right]\right\} \quad (3)$$

So, due to the following formulae (4) and (5),

$$\Phi=\oiint\vec{B}\overrightarrow{dS} \quad (4)$$

$$\mathcal{E}=-N\frac{d\Phi}{dt} \quad (5)$$

the voltage at the terminals of the flux sensor will contain harmonics of the following ranks due to the fault:

$$f_{ecc}=\left(n\pm\frac{k}{p}\right)\omega_s t \quad (6)$$

In both operating cases, the stray flux signal consists of the fundamental harmonic at 50 Hz and the third harmonic at 150 Hz (as seen in Figs. 13-16). However, the spectrograms of the faulty machine are richer in its harmonic index. Specifically, the $\frac{f_s}{p}, 2f_s$ and $5f_s$ appear in the low-frequency region close to the fundamental. It is to be noted that an additional harmonic trajectory at $3f_s-\frac{f_s}{p}$ is noticeable only in the faulty machine connected to the ohmic load bank. Finally, it is noteworthy that one more powerful harmonic dominates the spectrograms of the faulty machine at a frequency related to the slot number of the rotor of the brushless exciter and equal to $\frac{N_e}{p}f_s$ (equal to 750 Hz in this case).

Due to the dynamic oscillations of the shaft, the exciter is eccentric as well with respect to the stator. Therefore, it creates rotor slot harmonics similarly to those of the induction motor. Such harmonics are well-known for detecting dynamic eccentricity faults. In this case, the exciter slot harmonics significantly increase in the case of the faulty synchronous generator indicating a mechanical oscillation and variation of the magnetic reluctance between the stator core and the rotating exciter core.

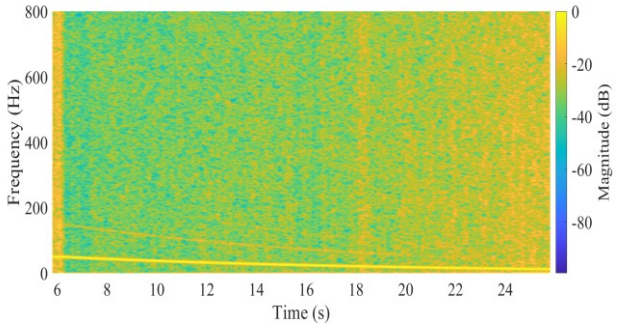

Fig. 13. Leakage stray flux (ϕ_l) STFT spectrogram when armature winding is open for the healthy machine.

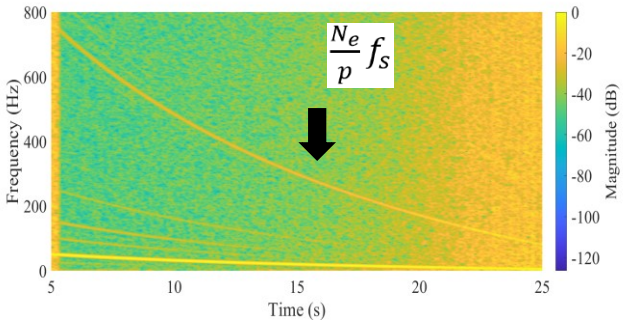

a)

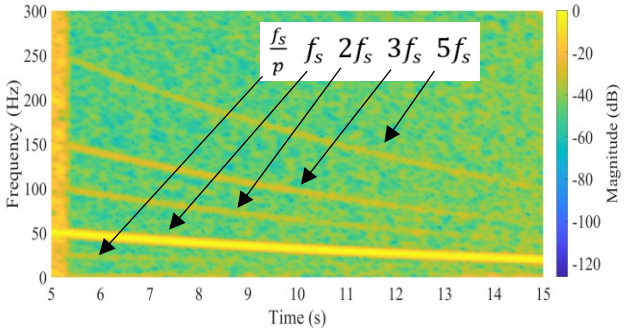

b)

Fig. 14. Leakage stray flux (ϕ_l) STFT spectrogram when armature winding is open for the faulty machine where upper plot depicts the full spectrogram and bottom plot provide a zoomed view at low frequencies.

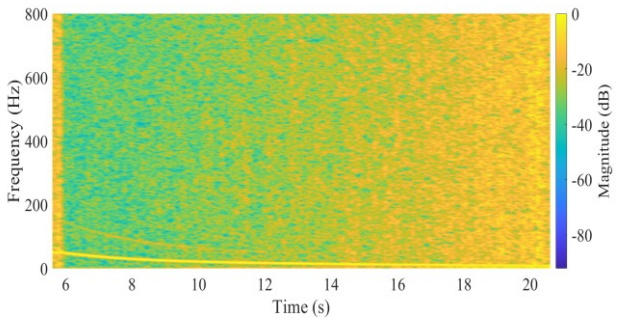

Fig. 15. Leakage stray flux (ϕ_l) STFT spectrogram when armature winding is feeding the ohmic load bank for the healthy machine.

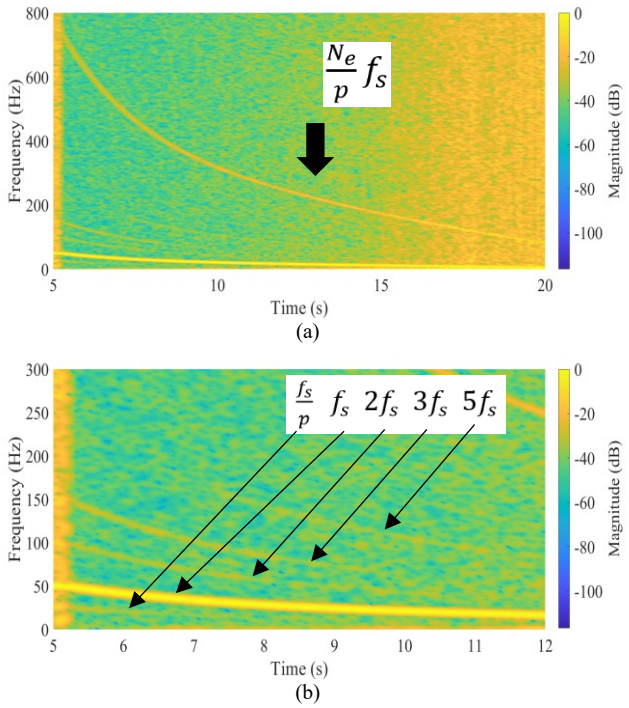

Fig. 16. Leakage stray flux (ϕ_l) STFT spectrogram when armature winding is feeding the ohmic load bank for the faulty machine where (a) full spectrogram and (b) zoom at low frequencies.

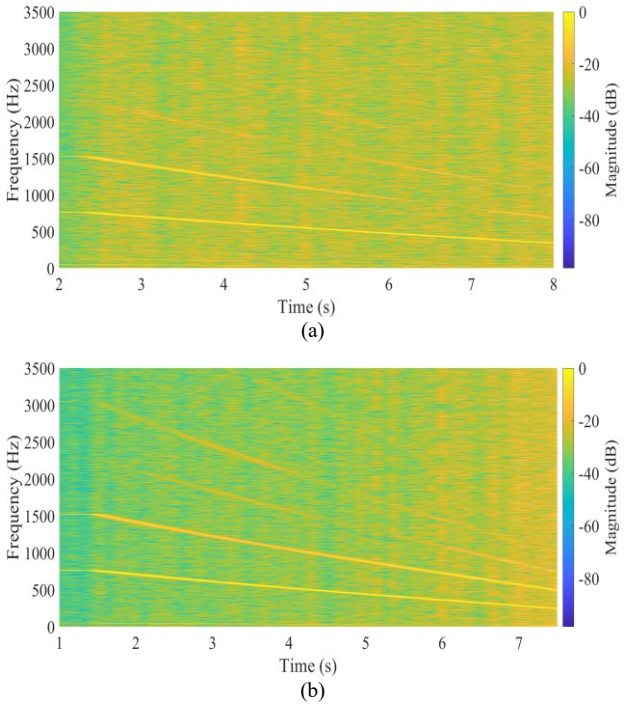

Fig. 17. Axial stray flux ($\phi_{l,z}$) STFT spectrogram when armature winding is feeding the ohmic load bank for the: (a) healthy and (b) faulty machine.

B. Axial Flux Monitoring Results and Analysis

The flux sensor has been placed on the side of the brushless exciter with its effective area perpendicular to the axial machine direction in order to capture purely axial flux. Radial flux machines are generally known to generate axial flux components in cases of asymmetries and faults. The STFT spectrograms are shown in the following Fig. 17 for both cases. It is clear that the components $\frac{N_e}{p} f_s$ and $2\frac{N_e}{p} f_s$ are clear in the healthy machine, while a very weak $3\frac{N_e}{p} f_s$ is also present, however, its trajectory is not fully visible.

On the other hand, the faulty machine demonstrates a series of the first 4 multiples of $\frac{N_e}{p} f_s$ very clearly and even a weaker trajectory of the $6\frac{N_e}{p} f_s$. Those higher harmonic components are the result of the asymmetrical EMF induced to the sensor due to the eccentric condition.

VI. Conclusion

This paper performs a multi-parametric condition monitoring of salient pole wound-field synchronous machines (WFSMs) equipped with a brushless exciter, which is based on an experimental investigation. The goal is to identify mechanical faults leading to eccentricity, such as a cocked bearing in this particular case. At steady-state, it is clear from the results that the MCSA has an advantage over the stray flux monitoring, which may have a high noise floor. In addition, the thermographic analysis proves that the cocked bearing on the prime mover end will also affect the bearing from the exciter end as well. It is also found that the fault's mechanical oscillations will lead to the induction of harmonics in the flux sensor that depend on the geometrical properties of the exciter. The contribution of this paper is the development of a new test scheme aiming to take advantage of that phenomenon, where the stray flux is recorded while the prime mover deaccelerates. The test can be applied while the generator is either under load or open-circuited. The spectrogram of the stray radial and axial flux proves to be sensitive to the mechanical fault's existence and offers very clear trajectories of relevant signatures. Future work will focus on the separation of different mechanical faults and their distinctive impact through this new methodology.

Acknowledgment

The authors would like to thank Mr Jamie Graham of the University of Edinburgh for his technical support of this work.

References

[1] J. K. Nøland, S. Nuzzo, A. Tessarolo and E. F. Alves, "Excitation System Technologies for Wound-Field Synchronous Machines: Survey of Solutions and Evolving Trends," in IEEE Access, vol. 7, pp. 109699-109718, 2019, doi: 10.1109/ACCESS.2019.2933493.

[2] C. Sun, W. Liu, Z. Wei, N. Jiao and J. Pang, "Open-Circuit Fault Diagnosis of Rotating Rectifier by Analyzing the Exciter Armature Current," in IEEE Transactions on Power Electronics, vol. 35, no. 6, pp. 6373-6385, June 2020, doi: 10.1109/TPEL.2019.2951431.

[3] M. Salah, K. Bacha, A. Chaari and M. E. H. Benbouzid, "Brushless Three-Phase Synchronous Generator Under Rotating Diode Failure Conditions," in IEEE Transactions on Energy Conversion, vol. 29, no. 3, pp. 594-601, Sept. 2014, doi: 10.1109/TEC.2014.2312173.

[4] Y. Wu, B. Cai and Q. Ma, "An Online Diagnostic Method for Rotary Diode Open-Circuit Faults in Brushless Exciters," in IEEE Transactions

on Energy Conversion, vol. 33, no. 4, pp. 1677-1685, Dec. 2018, doi: 10.1109/TEC.2018.2831241.

[5] S. Afrandideh, M. E. Milasi, F. Haghjoo and S. M. A. Cruz, "Turn to Turn Fault Detection, Discrimination, and Faulty Region Identification in the Stator and Rotor Windings of Synchronous Machines Based on the Rotational Magnetic Field Distortion," in IEEE Transactions on Energy Conversion, vol. 35, no. 1, pp. 292-301, March 2020, doi: 10.1109/TEC.2019.2951528.

[6] S. Afrandideh, F. Haghjoo, S. Cruz and M. Eshaghi Milasi, "Detection of Turn-to-Turn Faults in the Stator and Rotor of Synchronous Machines During Startup," in IEEE Transactions on Industrial Electronics, vol. 68, no. 8, pp. 7485-7495, Aug. 2021, doi: 10.1109/TIE.2020.3003626.

[7] M. E. Milasi, S. Afrandideh and F. Haghjoo, "A Simple Flux-Based Technique to Specify the Faulty Pole of the Salient Pole Synchronous Machines," in IEEE Transactions on Energy Conversion, vol. 36, no. 1, pp. 264-271, March 2021, doi: 10.1109/TEC.2020.3002260.

[8] H. Ehya, T. Skreien and A. Nysveen, "Intelligent Data-driven Diagnosis of Incipient Inter-turn Short Circuit Fault in Field Winding of Salient Pole Synchronous Generators," in IEEE Transactions on Industrial Informatics, doi: 10.1109/TII.2021.3054674.

[9] J. Yun et al., "Airgap Search Coil-Based Detection of Damper Bar Failures in Salient Pole Synchronous Motors," in IEEE Transactions on Industry Applications, vol. 55, no. 4, pp. 3640-3648, July-Aug. 2019, doi: 10.1109/TIA.2019.2912148.

[10] Y. Park, S. B. Lee, J. Yun, M. Sasic and G. C. Stone, "Air Gap Flux-Based Detection and Classification of Damper Bar and Field Winding Faults in Salient Pole Synchronous Motors," in IEEE Transactions on Industry Applications, vol. 56, no. 4, pp. 3506-3515, July-Aug. 2020, doi: 10.1109/TIA.2020.2983902.

[11] M. F. Shaikh, J. Park and S. B. Lee, "A Non-Intrusive Leakage Flux Based Method for Detecting Rotor Faults in the Starting Transient of Salient Pole Synchronous Motors," in IEEE Transactions on Energy Conversion, vol. 36, no. 2, pp. 1262-1270, June 2021, doi: 10.1109/TEC.2020.3021207.

[12] H. Ehya and A. Nysveen, "Comprehensive Broken Damper Bar Fault Detection of Synchronous Generators," in IEEE Transactions on Industrial Electronics, doi: 10.1109/TIE.2021.3071678.

[13] V. Gurusamy, G. -A. Capolino, B. Akin, H. Henao, R. Romary and R. Pusca, "Recent Trends in Magnetic Sensors and Flux Based Condition Monitoring of Electromagnetic Devices," in IEEE Transactions on Industry Applications, doi: 10.1109/TIA.2022.3174804.

[14] Ehsan Mazaheri-Tehrani,Jawad Faiz, "Airgap and stray magnetic flux monitoring techniques for fault diagnosis of electrical machines: An overview", IET Elec. Pow. Appl., Vol. 16, No. 3, pp. 277-299, 2022.

[15] S. B. Lee et al., "Condition Monitoring of Industrial Electric Machines: State of the Art and Future Challenges," in IEEE Industrial Electronics Magazine, vol. 14, no. 4, pp. 158-167, Dec. 2020, doi: 10.1109/MIE.2020.3016138.

[16] B. M. Ebrahimi, J. Faiz and M. J. Roshtkhari, "Static-, Dynamic-, and Mixed-Eccentricity Fault Diagnoses in Permanent-Magnet Synchronous Motors," in IEEE Transactions on Industrial Electronics, vol. 56, no. 11, pp. 4727-4739, Nov. 2009, doi: 10.1109/TIE.2009.2029577.

[17] R. Z. Haddad and E. G. Strangas, "On the Accuracy of Fault Detection and Separation in Permanent Magnet Synchronous Machines Using MCSA/MVSA and LDA," in IEEE Transactions on Energy Conversion, vol. 31, no. 3, pp. 924-934, Sept. 2016, doi: 10.1109/TEC.2016.2558183.

[18] S. T. Lee and J. Hur, ''Detection technique for stator inter-turn faults in BLDC motors based on third-harmonic components of line currents'', IEEE Transactions on Industry Applications, Vol. 53, No. 1, pp. 143–150, 2017.

[19] K. N. Gyftakis, S. Rasid, G. Skarmoutsos and M. A. Mueller, "The Demagnetization Harmonics Generation Mechanism in Permanent Magnet Machines with Concentrated Windings," in IEEE Transactions on Energy Conversion, doi: 10.1109/TEC.2021.3071598.

[20] S. Khojet El Khil, I. Jlassi, A. J. Marques Cardoso, J. O. Estima and N. Mrabet-Bellaaj, "Diagnosis of Open-Switch and Current Sensor Faults in PMSM Drives Through Stator Current Analysis," in IEEE Transactions on Industry Applications, vol. 55, no. 6, pp. 5925-5937, Nov.-Dec. 2019, doi: 10.1109/TIA.2019.2930592.

[21] A. Choudhary, D. Goyal and S. S. Letha, "Infrared Thermography-Based Fault Diagnosis of Induction Motor Bearings Using Machine Learning," in IEEE Sensors Journal, vol. 21, no. 2, pp. 1727-1734, 15 Jan.15, 2021, doi: 10.1109/JSEN.2020.3015868.

[22] M. Delgado-Prieto, J. A. Carino-Corrales, J. J. Saucedo-Dorantes, R. de Jesus Romero-Troncoso and R. A. Osornio-Rios, "Thermography-Based Methodology for Multifault Diagnosis on Kinematic Chain," in IEEE Transactions on Industrial Informatics, vol. 14, no. 12, pp. 5553-5562, Dec. 2018, doi: 10.1109/TII.2018.2816925.

[23] D. López-Pérez and J. Antonino-Daviu, "Application of Infrared Thermography to Failure Detection in Industrial Induction Motors: Case Stories," in IEEE Transactions on Industry Applications, vol. 53, no. 3, pp. 1901-1908, May-June 2017, doi: 10.1109/TIA.2017.2655008.

[24] K. N. Gyftakis, C. A. Platero and J. K. Nøland, "Multi-Parametric Monitoring of Medium-Power Generators with Brushless Exciters under Mechanical Faults," 2022 International Conference on Electrical Machines (ICEM), pp. 1524-1529, Valencia, Spain, 2022.

Konstantinos N. Gyftakis (M'11-SM'20) received the Diploma in Electrical and Computer Engineering from the University of Patras, Patras, Greece in 2010. He pursued a Ph.D in the same institution in the area of electrical machines condition monitoring and fault diagnosis (2010-2014). Furthermore, he worked as a Post-Doctoral Research Assistant in the Dept. of Engineering Science, University of Oxford, UK (2014-2015). Then he worked as Lecturer (2015-2018) and Senior Lecturer (2018-2019) in the School of Computing, Electronics and Mathematics and as an Associate with the Research Institute for Future Transport and Cities, Coventry University, UK. Finally, between 2019-2022, he worked as a Lecturer in Electrical Machines and a Member of the Institute for Energy Systems, University of Edinburgh, UK.

He is currently an Associate Professor with the School of Electrical and Computer Engineering, Technical University of Crete, Greece. His research interests focus in the fault diagnosis, condition monitoring and degradation of electrical machines. He has authored/co-authored more than 120 papers in international scientific journals and conferences Moreover, he is Secretary and International Steering Committee Member of the IEEE Symposium on Diagnostics for Electrical Machines, Power Electronics and Drives. Finally, he serves as an Associate Editor for the IEEE Transactions on Industry Applications and the IEEE Transactions on Energy Conversion.

Carlos A. Platero (M´10-SM´10) was born in Madrid, Spain, in 1972. He obtained the Dipl. degree and Ph.D. degree in electrical engineering from the Technical University of Madrid, Spain, in 1996 and 2007 respectively. Since 1996 to 2008 he has worked in ABB Generación S.A., Alstom Power S.A. and ENDESA Generación SA, always

involved in design and commissioning of power plants. In 2002 he began teaching at the Electrical Engineering Department of the Technical University of Madrid, and joined an energy research group. In 2008 he became full-time Associate Professor. During these years, he was working in protections, condition monitoring and diagnosis of electrical machines, especially large synchronous generators as well as integration of renewable energy in power systems through storage pumped power plants. He has been Visiting Professor in EPFL (Swiss Federal Institute of Technology Lausanne) 2012/2013/2014, Coventry University (U.K.) 2014/2016, and Edinburgh University (U.K.) 2019.

Jonas Kristiansen Nøland (S'14-M'17) was born in Drammen, Norway, in 1988. He received the M.Sc. degree in electric power engineering from the Chalmers University of Technology, Gothenburg, Sweden, in 2013, and the Ph.D. degree in engineering physics from Uppsala University, Uppsala, Sweden, in 2017. Since 2018, he has been an Associate Professor with the Department of Electric Power Engineering, Norwegian University of Science and Technology. His research interests include enhancing the utilization of wound-field synchronous machines and their excitation systems.

Dr. Nøland serves as an Associate Editor for the IEEE TRANSACTIONS ON ENERGY CONVERSION and the IEEE TRANSACTIONS ON INDUSTRIAL ELECTRONICS.